HHS Public Access

Author manuscript

Biochemistry. Author manuscript; available in PMC 2020 August 05.

Published in final edited form as:

Biochemistry. 2019 July 30; 58(30): 3251–3259. doi:10.1021/acs.biochem.9b00430.

Modulating Integrin αIIbβ3 Activity through Mutagenesis of Allosterically Regulated Intersubunit Contacts

Sophia K. Tan[†,‖], **Karen P. Fong**[‡,‖], **Nicholas F. Polizzi**[†], **Alex Sternisha**[‡], **Joanna S. G. Slusky**[§], **Kyungchul Yoon**[‡], **William F. DeGrado**[†], **Joel S. Bennett**[*,‡]

[†]Department of Pharmaceutical Chemistry, University of California, San Francisco, San Francisco, California 94158, United States

[‡]Hematology-Oncology Division, University of Pennsylvania School of Medicine, Philadelphia, Pennsylvania 19104, United States

[§]Department of Molecular Biosciences and Center for Computational Biology, University of Kansas, Lawrence, Kansas 66045, United States

Abstract

Integrin αIIbβ3, a transmembrane heterodimer, mediates platelet aggregation when it switches from an inactive to an active ligand-binding conformation following platelet stimulation. Central to regulating αIIbβ3 activity is the interaction between the αIIb and β3 extracellular stalks, which form a tight heterodimer in the inactive state and dissociate in the active state. Here, we demonstrate that alanine replacements of sensitive positions in the heterodimer stalk interface destabilize the inactive conformation sufficiently to cause constitutive αIIbβ3 activation. To determine the structural basis for this effect, we performed a structural bioinformatics analysis and found that perturbing intersubunit contacts with favorable interaction geometry through substitutions to alanine quantitatively accounted for the degree of constitutive αIIbβ3 activation. This mutational study directly assesses the relationship between favorable interaction geometry at mutation-sensitive positions and the functional activity of those mutants, giving rise to a simple model that highlights the importance of interaction geometry in contributing to the stability between protein−protein interactions.

Graphical abstract

[*]**Corresponding Author** Hematology-Oncology Division, Department of Medicine, Perelman School of Medicine, University of Pennsylvania, Philadelphia, PA 19104. Telephone: 215-573-3280. Fax: 215573-7039. bennetts@pennmedicine.upenn.edu.

[‖] S.K.T. and K.P.F. contributed equally to this work.

ASSOCIATED CONTENT

Supporting Information

The Supporting Information is available free of charge on the ACS Publications website at DOI: 10.1021/acs.biochem.9b00430.

Tables S1 and S2 and Figure S1 (PDF)

Accession Codes

PDB entry 3FCS: chains A (residues 599–959) and B (residues 483–690) of the αIIbβ3 crystal structure.

The authors declare no competing financial interest.

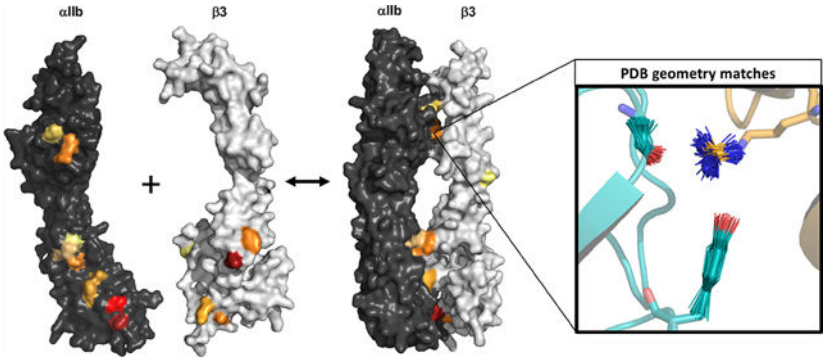

Integrin αIIbβ3 resides on the platelet surface in a regulated and finely tuned equilibrium between resting low-affinity and active high-affinity conformations that can be perturbed by bidirectional signal transduction.[1] Crystal structures of resting αIIbβ3 have revealed that its extracellular domain has a bent conformation with its nodular ligand-binding headpiece oriented toward the cell surface[2,3] and with contacts between the β3 and αIIb stalks forming a clasp that maintains its inactive state (Figure 1).[4] Following platelet stimulation, αIIbβ3 undergoes a global rearrangement5 in which its ligand-binding headpiece turns away from the cell surface and its transmembrane (TM) and stalk domains separate. This causes the integrin to shift to a fully extended conformation,[6] exposing its ligand-binding site. *In vivo*, intracellular signals shift αIIbβ3 toward its high-affinity ligand-binding conformation ("inside-out signaling").[7] However, αIIbβ3 can also be experimentally shifted to its active conformation by replacing individual amino acids in its TM or membrane-proximal extracellular stalk domains, although the magnitude of the shift varies from replacement to replacement.

In this study, we characterized the αIIbβ3 stalk interface by introducing alanine replacements and measuring their effects on constitutive integrin activation. Protein−protein interfaces, such as the interface between the αIIb and β3 stalks, are usually large complementary surfaces with many intermolecular contacts.[8] Nonetheless, as Clackson and Wells pointed out,[9] a limited number of complementary side chain interactions in protein −protein interfaces, termed "hot spots", are disproportionately responsible for the strength of binding. Previously, we used the Rosetta alanine scanning algorithm to identify hot spots in the β3 stalk and found that replacing them with alanine was sufficient to activate both αIIbβ3 and αvβ3.[10] However, while the alanine scanning algorithm successfully predicted mutations that destabilized the stalk interface, it did not correctly rank their functional effects, likely because the energetic effects of the alanine substitutions were weak and within the margin of error reported for this method.[11]

Here, we sought to identify hot spots in the αIIb stalk that are complementary to those we previously identified in β3. Initially, we scanned the αIIb Calf-1 and Calf-2 domains using the Rosetta-based alanine scanning algorithm and subsequently using the recently described Rosetta flex ddG protocol.[12] The latter enables more accurate $\Delta\Delta G$ predictions by generating ensembles of models sampling different backbone conformations, whereas the former does not. However, neither method was able to accurately predict the relative

contribution of the identified hot spots to the stability of the αIIbβ3 stalk complex. Therefore, to more precisely map the αIIbβ3 stalk interface, we developed a structural bioinformatics method based on the premise that the detailed geometries of the most stabilizing intersubunit side chain−side chain interactions would be overrepresented in the Protein Data Bank (PDB). We used the results of this analysis to compute an interaction geometry score that was better able to rationalize the nature of destabilizing mutations in the stalk interface than the flex ddG protocol. In addition, we found that specific stalk domain hot spots are responsible for maintaining the inactive state of αIIbβ3. Because the stalks are present in an extracellular location, these results suggest that stabilizing the stalk heterodimers may be a way to allosterically attenuate αIIbβ3 function.

METHODS

Computational Alanine Scanning Using Rosetta-Based Scanning Algorithms.

For all of our computational analyses, we used chains A (residues 599–959) and B (residues 483–690) from the αIIbβ3 crystal structure (PDB entry 3FCS).[4] We initially used Rosetta interface alanine scanning, hosted on the Robetta server, to predict hot spots in the αIIb stalk.[11,13] After completing the experimental aspects of this work, we repeated the computational alanine scanning mutagenesis using flex ddG, a recently developed method built within the Rosetta macromolecular modeling suite that provides more accurate $\Delta\Delta G$ predictions by generating ensembles of models that sample over different backbone and side chain conformations.[12] $\Delta\Delta G$ predictions were calculated using the hyperparameters recommended in the flex ddG tutorial Github repository (https://github.com/Kortemme-Lab/flex_ddG_tutorial). Briefly, ensembles of wild-type (WT) and alanine mutant models were generated by sampling 35000 backrub backbone perturbation (“backrub”) and minimization cycles. $\Delta\Delta G$’s between WT and alanine mutants were calculated using Rosetta energy function terms that were reweighted to better fit experimental $\Delta\Delta G$’s reported in the ZEMu protein−protein interaction benchmark set.[12,14]

Stable Expression of αIIbβ3 in Chinese Hamster Ovary (CHO) Cells.

Full-length cDNAs for human αIIb and β3 were inserted into pcDNA3.1(+) Neo and pcDNA3.1(+) Zeo (Invitrogen), respectively. Single-amino acid substitutions were introduced into the αIIb cDNA by polymerase chain reaction (PCR) using the QuickChange Site-Directed Mutagenesis Kit (Stratagene). The forward and reverse primers for the PCR are listed in Table S1. All mutated sequences were confirmed by DNA sequence analysis.

CHO cells were cultured in Ham’s F-12 medium (Gibco/ BRL) supplemented with 10% fetal bovine serum (Hyclone Laboratories). Plasmids containing cDNAs for WT and mutant αIIb and β3 were introduced into the CHO cells using FuGENE 6 according to the manufacturer’s instructions (Roche Molecular Biochemicals). Two days after being transfected, the cells were transferred to selection medium containing 500 μg/mL G418 (Gibco/BRL) and 300 μg/mL Zeocin (Invitrogen). After selection for 3 weeks, αIIbβ3 expression was assessed by flow cytometry using A2A9, a monoclonal antibody (mAb) that recognizes the human αIIbβ3 heterodimer.[15] Transfected cells were then repeatedly sorted

by fluorescence-activated cell sorting to obtain subclones expressing comparable high levels of WT and mutant αIIbβ3.

Fibrinogen Binding to CHO Cells Expressing αIIbβ3.

Fibrinogen binding to CHO cell subclones expressing comparable amounts of WT and mutant αIIbβ3 was measured as described previously.[16] Briefly, CHO cells (2×10^6 cells/mL) were incubated with the β3 mAb SSA6 conjugated to Alexa Fluor 647 (Invitrogen) to label αIIbβ3 and freshly prepared 5 mM dithiothreitol (DTT) with or without 2 mM EDTA for 15 min at 37 °C. The labeled cells were then incubated for 15 min at 37 °C with 200 μg/mL fibrinogen conjugated with Alexa Fluor 488 (Molecular Probes). Cells were washed, fixed with 4% paraformaldehyde in phosphate-buffered saline (PBS), and examined by two-color fluorescence-activated cell sorting analysis. Fibrinogen specifically bound to αIIbβ3 was defined as fibrinogen binding that was inhibited by EDTA. Statistical analyses of the fibrinogen binding data were performed using Microsoft Excel for Mac.

Specific fibrinogen binding data were used to calculate an αIIbβ3 activation index (AI), defined by eq 1:

$$\mathrm{AI} = (\mathrm{FB_c} - \mathrm{FB_{c+EDTA}})/(\mathrm{FB_{DTT}} - \mathrm{FB_{DTT+EDTA}}) \quad (1)$$

where $\mathrm{FB_c}$ represents fibrinogen binding to αIIbβ3 in the absence of an activating agent; $\mathrm{FB_{DTT}}$, fibrinogen binding to αIIbβ3 induced by 5 mM DTT; $\mathrm{FB_{c+EDTA}}$, constitutive fibrinogen binding to αIIbβ3 in the presence of 2 mM EDTA; and $\mathrm{FB_{DTT+EDTA}}$, fibrinogen binding to αIIbβ3 induced by 5 mM DTT in the presence of 2 mM EDTA. Because we extended our analysis to include the β3 stalk domain mutants we characterized in our previous work,[10] to maintain consistency, we converted the fibrinogen binding data to the apparent free energy of fibrinogen binding (ΔG_{app}) as defined by eq 2:

$$\Delta G_{\mathrm{app}} = -RT\ln\left(\frac{\text{activation index}}{1 - \text{activation index}}\right) \quad (2)$$

Database Curation of Nonredundant Protein Structures To Query Interaction Motifs.

To rationalize the strengths of αIIbβ3 mutant stalk interactions, we developed a structural bioinformatics analysis method based on the hypothesis that disrupting αIIb and β3 stalk interactions that are over-represented in the PDB[17] would destabilize the resting αIIbβ3 heterodimer and hence activate αIIbβ3. We curated a data set of crystallographic structures from the PDB (accessed February 7, 2018) with ≤30% sequence identity, ≤2 Å resolution, an R value of ≤0.3, and a MolProbity[18] score of <2 to evaluate clashing and rotamer/ϕ/ψ geometry, resulting in a database of 8415 structures. Biological assemblies were then reconstructed using ProDy[19] to maintain interactions across different monomers.

Decomposition of Hot Spot Interactions into Fragments for Database Searching.

Next, we discretized putative hot spot interactions into fragments to query our nonredundant PDB data set for the same interaction geometry between fragments. For each putative hot spot residue with experimentally derived functional data, we determined its opposite subunit

interacting fragments using the program Probe,[20] first minimizing the αIIbβ3 crystal structure using Rosetta's minimize_ppi application.[21,22] Each intersubunit contact Probe classified as a hydrogen bond, close contact, or strong atomic overlap was discretized into fragments belonging to a single residue that could fall within a plane. Fragments from side chains with tetrahedral geometry were limited to three atoms if the fragment contained an sp^3-hybridized carbon, while fragments could contain at least three atoms if one or more atoms were sp^2-hybridized or aromatic. Fragments from a single residue could also arise from backbone atoms ([N, CA, C] or [CA, C, O]). For example, aspartic acid fragments could be [N, CA, C], [CA, C, O], [N, CA, CB], [C, CA, CB], [CA, CB, CG], or [CB, CG, OD1, OD2]. However, we evaluated the interaction geometry for backbone fragments only if they originated from a complementary subunit residue rather than a putative hot spot residue, because interactions from backbone fragments of a hot spot residue would not be eliminated upon mutating the hot spot residue to alanine.

Database Search for Geometric Matches of Integrin Interactions.

To determine the favorability of the intersubunit interactions, we searched the nonredundant protein data set for residue pairs that had fragments interacting in the same geometry as in the WT crystal structure (PDB entry 3FCS). For each interaction between a hot spot residue AA_h and its complementary residue, AA_i, we approximated the energetic contribution imparted by forming an interaction in that specific geometry as Geom(h). This term was defined as the observed fraction of database AA_h interactions with AA_i occurring in the same geometry as in the αIIbβ3 crystal structure, normalized by the expected fraction of residue AA_h coming into contact with AA_i if there were no geometrical preference for the interaction. The observed fraction of AA_h interactions with AA_i that were geometric matches to the αIIbβ3 crystal structure was defined as the number of database residue pairs whose fragments could be superimposed onto the interacting fragments in the αIIbβ3 crystal structure with a 0.5 Å root-mean-square deviation ($M_{[\mathrm{frag}\alpha\mathrm{II}\beta,\ \mathrm{frag}\beta3]_{\mathrm{integrin}}}$), normalized by the total number of AA_h–AA_i residue pairs in the database $\{M[AA(\mathrm{frag}\alpha\mathrm{II}\beta),\mathrm{AA}(\mathrm{frag}\beta3)]\}$. The expected frequency of this pairwise interaction, assuming no preference for geometry, was defined as the product of the independent frequencies of each amino acid occurring in the database (denominator in eq 3). To account for residue pairs that were in contact simply because of sequence proximity, and not necessarily because of favorable interactions, we included only residue pairs on the same chain if they were separated by at least 10 residues. Calculations were performed using the Python package NumPy,[23] and plots were created using the Python package Matplotlib.[24]

$$\mathrm{Geom}(h) = \sum_{\left(\mathrm{frag}_{\mathrm{glip}}\mathrm{frag}_{33}\right)} -RT \times \ln\left\{\frac{M_{\left[\mathrm{frag}_{\mathrm{cllp}},\mathrm{frag}_{\beta3}\right]_{\mathrm{integin}}}/N_{\left[\mathrm{AA}\left(\mathrm{frag}_{\mathrm{aII}\beta}\right),\ \mathrm{AA}\left(\mathrm{frag}_{\beta3}\right)\right]}}{f_{\left[\mathrm{AA}\left(\mathrm{frag}_{\mathrm{all}\beta}\right)\right]}f_{\left[\mathrm{AA}\left(\mathrm{frag}_{\beta3}\right)\right]}}\right\} \quad (3)$$

Molecular Model of the Distal αIIbβ3 Stalk.

The stalk domains of αIIbβ3were modeled using the molecular visualization tool PyMOL (The PyMol Molecular Graphics System, version 2.0, Schrödinger, LLC) and the X-ray

diffraction crystal structures of αIIbβ3 obtained from the RCSB Protein Data Bank [entry 3FCS (https://www.ncbi.nlm.nih.gov/pubmed/19111664)]. The αIIbβ3 stalk domain model encompassed αIIb residues 599–959 and β3 residues 483–691.

RESULTS

Computational Alanine Scanning of the αIIb Calf-1 and Calf-2 Domains Identifies Mutation-Sensitive Residues.

Crystal structures of the ectodomain of inactive αIIbβ3 revealed a large interface between the Calf-1 and Calf-2 domains of the αIIb stalk and the EGF-3, EGF-4, and βTD domains of the distal β3 stalk[4,25] (Figure 1). Previously, we used the Robetta alanine scanning algorithm to predict destabilizing alanine replacements in the β3 stalk and found that introducing these replacements into full-length αIIbβ3 caused constitutive αIIbβ3 activation.[10] Using the same method to determine hot spots in the αIIb stalk, we identified 12 alanine replacements with predicted $\Delta\Delta G$'s ranging from 0.1 to 1.8 kcal/mol (Table 1). To determine which replacements destabilized the interface of the stalk sufficiently to cause αIIbβ3 activation, we introduced 10 of the replacements into full-length αIIb by site-directed mutagenesis, stably co-expressed the mutants with WT β3 in CHO cells, and measured both constitutive and dithiothreitol-induced fibrinogen binding to subclones selected by fluorescence-activated cell sorting analysis for comparable expression of αIIbβ3. To ensure that results were not unique to a particular subclone, fibrinogen binding measurements were performed using two to six different subclones. To normalize the activity of the various αIIbβ3 mutants, we calculated an αIIbβ3 activation index, the ratio of constitutive fibrinogen binding to αIIbβ3 to maximal fibrinogen binding induced by dithiothreitol. The R751A mutant was not expressed, implying that R751 may be important for either correct αIIb folding or correct αIIbβ3 assembly. Each of the other mutants was expressed to a comparable extent and caused a variable degree of constitutive αIIbβ3 activation, with αIIbβ3 activation indices ranging from 0.83 ± 0.12 for V760A to 0.17 ± 0.02 for H787A (Table 1).

Mapping Experimentally Determined Activation Indices onto the Structure of the αIIbβ3 Stalk Reveals the Relative Positioning and Molecular Contacts of Hot Spot and Neutral Residues.

We then mapped the hot spots we identified in αIIb, and those we previously identified in β3,[10] onto the model of the stalk heterodimer shown in Figure 2. Hot spot residues whose alanine mutants promoted αIIbβ3 activation were found to lie along a discontinuous strip running through the stalk interface. In the assembled stalk heterodimer, residues having high activation indices when replaced with alanine (i.e., ≥0.4) were flanked by hot spot residues whose alanine mutants activate αIIbβ3 to a lesser extent. By contrast, β3 residues D552 and H626, chosen as negative controls because they do not make intersubunit contacts with αIIb, were predicted to have no effect on αIIbβ3 heterodimer stability[10] and did not cause constitutive αIIbβ3 activation (Table 1).

Computational Alanine Scanning Algorithms Inaccurately Capture the Energetics of αIIbβ3 Stalk Mutations.

As we previously observed for the β3 stalk,[10] the Robetta alanine scanning algorithm did not correctly rank the functional importance of the hot spots it predicted in the αIIb stalk (Figure S1). Because the recently reported flex ddG algorithm calculates more accurate $\Delta\Delta G$'s,[12] we repeated the computational alanine scanning using the newer method. To comprehensively examine the whole stalk interface, we extended our analysis to include the β3 mutants characterized in our previous work.[10] When we plotted the apparent free energy of binding (ΔG_{app}) of fibrinogen to mutant αIIbβ3 versus the $\Delta\Delta G$'s predicted by flex ddG, we again found only a weak correlation (Figure 3A; $R^2 = 0.000$), likely because the energetic differences between the integrin mutants are within a very small range. The largest and smallest activation indices for the αIIbβ3 mutants differ by a factor of only 4.8, corresponding to an energetic change of only 1−2 kcal/mol, close to the expected flex ddG error of ±0.96 kcal/mol.[12]

Hot Spot Residues with High Activation Indices Interact with Complementary Residues in Geometries That Are Prevalent in the PDB.

To more accurately assess the energetic contribution of individual αIIb and β3 residues to the stability of resting αIIbβ3, we investigated whether hot spot residues impart stability in a predictable manner that could be ascertained by evaluating their interaction geometry. For each αIIb or β3 residue whose alanine mutant was experimentally characterized, we identified the complementary residues with which it interacted and represented the interaction as single-residue fragment pairs so that we could query the nonredundant PDB for pairs of fragments that interact in the same geometry as in the αIIbβ3 crystal structure. The nonredundant data set was then searched for geometric matches to WT αIIbβ3, which we defined as residue pairs whose fragments had a low root-mean-square deviation (≤0.5 Å) with the interacting fragment pairs in the αIIbβ3 crystal structure.

As anticipated, hot spot residues with high activation indices interacted with complementary subunit residues in geometries that are highly represented in the nonredundant PDB. Details of these interactions are shown in Figure 4 and listed in Table S2. For example, the hot spot residues whose alanine mutants have the highest activation indices, β3 T603 and αIIb V760, have numerous geometric matches. T603, whose activation index is 0.86, has a total of 385 geometric matches with six fragments on four αIIb residues. V760, whose activation index is 0.83, has 2940 geometric matches with one residue on β3. By contrast, αIIb residue I673, whose activation index is 0.23, has only 54 geometric matches. Mutants that do not cause integrin activation relative to WT (i.e., β3 D552A and β3 H626A) do not make any intersubunit interactions and have zero geometric matches in the PDB.

Figure 2. Mapping of functional hot spots identified by alanine scanning mutagenesis onto the structures of the αIIb and β3 stalk domains. The locations of residues in the distal αIIb and β3 stalk domains for which alanine replacements caused constitutive αIIbβ3 activation were mapped onto the structures for these domains and are color-coded according to the apparent free energy of fibrinogen binding (ΔG_{app}) of their alanine replacement (Table 1), as shown in the heat map below the models.

Quantitative Analysis of Interaction Geometry.

On the basis of our findings that frequently represented interaction geometries are present at the αIIbβ3 stalk interface, we developed a simple scoring function, Geom(*h*), to score the geometric interaction propensities of hot spot residue h (eq 3). We found a strong correlation between the Geom(*h*) score of a residue and the ability of its alanine replacement to cause αIIbβ3 activation. The Geom(*h*) scores for strongly activating β3 T603 and αIIb V760 were −3.75 and −2.91, respectively, while those for less activating αIIb residues I673 and N753 were 0.16 and −1.87, respectively. When we examined the quantitative agreement between the Geom(*h*) scores and the apparent energies of binding to fibrinogen, we found the correlation coefficient to be 0.796 (Figure 3B).

Nonetheless, there were two notable discrepancies between the computational alanine scanning and the structural bioinformatics results. First, αIIb S758 makes no direct interchain contacts, but its alanine replacement has a high activation index of 0.64. However, the αIIbβ3 crystal structure is not well-resolved in this region, as evidenced by the side chains of Q954/L956 of αIIb and K612/K658 of β3 not being represented in the electron density maps. Moreover, there is unassigned density corresponding to two volumes that could potentially be in contact with S758, suggesting that there may be solvent-mediated interchain interactions for which the bioinformatics method does not account (Figure 4).

The second exception is β3 E534. Previously, using Robetta alanine scanning, we predicted that E534A was moderately destabilizing with a $\Delta\Delta G$ of 0.54 kcal/mol.[10] On the basis of the crystal structure of inactive αIIbβ3, β3 E534A does not disrupt an interaction across the αIIbβ3 stalk interface. Rather, it disrupts a hydrogen bond between the β3 EGF-3 domain and the αIIb β-propeller located in the αIIb ectodomain (Figure 5), causing constitutive αIIbβ3 activation with an activation index of 0.76 ± 0.07. The structural bioinformatics analysis revealed that E534 interacts with β-propeller residue R402 with a Geom(*h*) score of −1.19, an intermediate degree of geometric favorability relative to the stalk mutants. However, E534A is more activating than its geometry score would suggest. Thus, while these results confirm that the structural bioinformatics method can describe favorable interaction geometries across different regions in multidomain proteins, it also cautions that without carefully training the model on a large database of interdomain interactions, we can rank only the favorability of those interactions within the same interface. E534 is also noteworthy because Zang and Springer had previously reported that mutating β2 residue Q535, analogous to β3 E534, as well as β2 V526, both located in the β2 EGF-3 domain, caused the activation of leukocyte integrin αxβ2 (CD11c/CD18) and postulated that an interaction between these residues and unidentified residues in αx restrained αxβ2 in its inactive state.[25] Our results suggest that the inactive state of αxβ2 is stabilized through an interaction similar to the β3 E534−αIIb R402 interaction and further support the bent conformation as a biologically relevant state for this class of integrins.

DISCUSSION

Platelets circulate in a milieu that is rich in fibrinogen, the principal ligand for integrin αIIbβ3. Because binding of fibrinogen to activated αIIbβ3 causes platelet aggregation, αIIbβ3 on circulating platelets is held in an inactive state by an intramolecular clasp

composed of portions of its cytosolic, TM, and extracellular stalk domains to prevent the formation of intravascular platelet aggregates.[26−28] At sites of vascular injury where rapid platelet aggregation is required to stop bleeding, platelet stimulation causes disruption of the clasp, followed by a global αIIbβ3 rearrangement during which its ectodomain extends and exposes its fibrinogen-binding site.[5]

In crystal structures[2,3] and electron microscope images[5,29] of the extracellular domain of inactive αIIbβ3, the lower leg of β3 is in the proximity of both the lower α leg and the integrin headpiece. One proposed trigger for the global rearrangement is the release of intersubunit contacts located in the stalk domain, thereby allowing the αIIb and β3 components of the stalk to separate and the ectodomain to extend.[30,31] Lending support for this mechanism, three families with the inherited bleeding disorder Glanzmann thrombasthenia have been reported in whom deletion of β3 residues D647−E686[32] or β3 residues D621−E660,[33] containing the predicted β3 hot spots K658 and V644, caused constitutive αIIbβ3 activation. Previously, Kamata et al. also reported that swapping the Calf2 domains of αIIb and αv enhanced Mn^{2+}-induced fibrinogen binding to αIIbβ3 but suppressed Mn^{2+}-induced fibrinogen binding to αvβ3, suggesting that the interface between the αsubunit Calf-2 domain and the β3 EGF-4 and βTD domains regulates Mn^{2+}-induced ligand binding to αIIbβ3 and αvβ3.[34] Consistent with this conclusion, Mn^{2+}-induced fibrinogen binding to αIIbβ3 was suppressed by an artificial disulfide bridge between the αIIb Calf-2 and β3 βTD domains. However, neither the Calf-2 domain swaps nor subsequent residue interchanges caused integrin activation in the absence of Mn^{2+}. Mn^{2+} by itself is a weak integrin activator, and neither the αIIb Calf-2 nor the β3 EGF-4-βTD domains bind cations. Thus, it is likely that perturbations in the interface between the α-and β-subunit stalks introduced by the Calf-2 domain swaps potentiated an effect of Mn^{2+} elsewhere in the αIIbβ3 and αvβ3 molecules. It has also been proposed that in bent integrins, the CD loop of the β3 βTD domain contacts the β3 βA domain F/α_7 loop, acting as a “deadbolt” to prevent the allosteric movement of the α7 helix that initiates opening of the integrin headpiece.[35] However, neither deleting nor mutating the CD loop perturbs ligand binding to αIIbβ3,[36] making it doubtful that these CD loop interactions regulate integrin function.

To identify hot spot interactions in the αIIb and β3 stalks that regulate αIIbβ3 function, we used the computational alanine scanning algorithm hosted on Robetta to predict interacting hot spots in the stalk heterodimer, initially identifying nine alanine replacements in β3[10] and then 12 alanine replacements in αIIb with predicted ΔΔG’s ranging from 0.06 to 2.89 kcal/mol. Hot spots have been variably defined as residues whose replacement by alanine destabilizes a protein−protein interface by ΔΔ*G*’s ranging from >1.0 to >4.0 kcal/mol.[8,9,11,37] It is noteworthy that only 8 of 21 alanine replacements had a predicted ΔΔG of >1.0 kcal/mol (Table 1), a proposed threshold for a destabilizing alanine replacement.[11,13] Furthermore, there was only a weak correlation (R^2 = 0.35) between the ΔΔ*G*’s predicted by the Robetta algorithm and the extent of αIIbβ3 activation that occurred when the alanine replacement was introduced into αIIbβ3 (Figure S1).

The recently reported flex ddG protocol generates ensembles of structures using the “backrub” protocol in Rosetta, thereby accounting for mutation-induced local side chain and

backbone conformational changes. Flex ddG has been found to outperform other existing computational methods that also sampled conformational space, particularly for small to large mutations. Nonetheless, there still was only a weak correlation between flex ddG and the energy of fibrinogen binding to αIIbβ3 (Figure 3A) because the effects we measured were small and within the margin of error of flex ddG.

To better understand the structural basis for αIIbβ activation, we developed a structural bioinformatics approach to analyze functionally important contacts in both the αIIb and β3 stalks. This approach was based on the hypothesis that functional groups have preferences in the relative position, orientation, and angles at which they interact, and these preferences are reflected in the PDB. Analyses of side chain interactions in the PDB have shown that propensities of these interactions deviate from the distributions expected from random packing, implying that side chain interactions are guided by directional preferences.[38−40] Taking this into account, we approximated the energetic contribution of a hot spot residue by identifying its interacting fragment pairs and querying the PDB for the prevalence of those interaction geometries. We found a strong correlation between our interaction geometry term and the binding energy of fibrinogen to αIIbβ3 (R^2 = 0.796) (Figure 3B). Thus, this approach shows promise for analyzing putative hot spots identified by alanine scanning. However, a much larger data set would need to be examined, and the choice of molecular interaction fragments would likely need to be optimized to generalize this method over a wide range of molecular interactions. Nonetheless, the ability to assess favorable interaction geometry through a knowledge-based method precludes the need to directly model mutation-induced structural changes as well as the need to directly calculate energetic effects. Ultimately, the interaction geometry metric can be incorporated into Rosetta, facilitating analysis of interaction geometry for interface evaluation and design.

Supplementary Material

Refer to Web version on PubMed Central for supplementary material.

ACKNOWLEDGMENTS

This work was supported by National Institutes of Health Grants P01 HL40387 (J.S.B. and W.F.D.) and R35 GM122603 (W.F.D.) as well as National Science Foundation (NSF) Grant 1709506 (W.F.D.). S.K.T. is supported by the NSF under Grant 1650113.

REFERENCES

(1). Li W, Metcalf DG, Gorelik R, Li R, Mitra N, Nanda V, Law PB, Lear JD, Degrado WF, and Bennett JS (2005) A push-pull mechanism for regulating integrin function. Proc. Natl. Acad. Sci. U. S. A 102, 1424–1429. [PubMed: 15671157]

(2). Xiong JP, Stehle T, Diefenbach B, Zhang R, Dunker R, Scott DL, Joachimiak A, Goodman SL, and Arnaout MA (2001) Crystal structure of the extracellular segment of integrin aVb3. Science 294, 339–345. [PubMed: 11546839]

(3). Xiao T, Takagi J, Coller BS, Wang JH, and Springer TA (2004) Structural basis for allostery in integrins and binding to fibrinogen-mimetic therapeutics. Nature 432, 59–67. [PubMed: 15378069]

(4). Zhu J, Luo BH, Xiao T, Zhang C, Nishida N, and Springer TA (2008) Structure of a complete integrin ectodomain in a physiologic resting state and activation and deactivation by applied forces. Mol. Cell 32, 849–861. [PubMed: 19111664]

(5). Takagi J, Petre B, Walz T, and Springer T. (2002) Global conformational rearrangements in integrin extracellular domains in outside-in and inside-out signaling. Cell 110, 599–611. [PubMed: 12230977]

(6). Luo BH, Carman CV, and Springer TA (2007) Structural basis of integrin regulation and signaling. Annu. Rev. Immunol 25, 619–647. [PubMed: 17201681]

(7). Shattil SJ, and Newman PJ (2004) Integrins: dynamic scaffolds for adhesion and signaling in platelets. Blood 104, 1606–1615. [PubMed: 15205259]

(8). Bogan AA, and Thorn KS (1998) Anatomy of hot spots in protein interfaces. J. Mol. Biol 280, 1–9. [PubMed: 9653027]

(9). Clackson T, and Wells JA (1995) A hot spot of binding energy in a hormone-receptor interface. Science 267, 383–386. [PubMed: 7529940]

(10). Donald JE, Zhu H, Litvinov RI, DeGrado WF, and Bennett JS (2010) Identification of interacting hot spots in the beta3 integrin stalk using comprehensive interface design. J. Biol. Chem 285, 38658−38665.

(11). Kortemme T, Kim DE, and Baker D. (2004) Computational alanine scanning of protein-protein interfaces. Sci. Signaling 2004, p l2.

(12). Barlow KA, O'Conchúir S, Thompson S, Suresh P, Lucas JE, Heinonen M, and Kortemme T. (2018) Flex ddG: Rosetta Ensemble-Based Estimation of Changes in Protein-Protein Binding Affinity upon Mutation. J. Phys. Chem. B 122, 5389–5399. [PubMed: 29401388]

(13). Kortemme T, and Baker D. (2002) A simple physical model for binding energy hot spots in protein-protein complexes. Proc. Natl. Acad. Sci. U. S. A 99, 14116−14121.

(14). Dourado DF, and Flores SC (2014) A multiscale approach to predicting affinity changes in protein-protein interfaces. Proteins: Struct., Funct., Genet 82, 2681–2690. [PubMed: 24975440]

(15). Bennett JS, Hoxie JA, Leitman SF, Vilaire G, and Cines DB (1983) Inhibition of fibrinogen binding to stimulated human platelets by a monoclonal antibody. Proc. Natl. Acad. Sci. U. S. A 80, 2417–2421. [PubMed: 6302680]

(16). Zhu H, Metcalf DG, Streu CN, Billings PC, Degrado WF, and Bennett JS (2010) Specificity for homooligomer versus heterooligomer formation in integrin transmembrane helices. J. Mol. Biol 401, 882–891. [PubMed: 20615419]

(17). Berman HM, Westbrook J, Feng Z, Gilliland G, Bhat TN, Weissig H, Shindyalov IN, and Bourne PE (2000) The Protein Data Bank. Nucleic Acids Res. 28, 235–242. [PubMed: 10592235]

(18). Chen VB, Arendall WB 3rd, Headd JJ, Keedy DA, Immormino RM, Kapral GJ, Murray LW, Richardson JS, and Richardson DC (2010) MolProbity: all-atom structure validation for macromolecular crystallography. Acta Crystallogr., Sect. D: Biol. Crystallogr 66, 12–21. [PubMed: 20057044]

(19). Bakan A, Meireles LM, and Bahar I. (2011) ProDy: protein dynamics inferred from theory and experiments. Bioinformatics 27, 1575–1577. [PubMed: 21471012]

(20). Word JM, Lovell SC, LaBean TH, Taylor HC, Zalis ME, Presley BK, Richardson JS, and Richardson DC (1999) Visualizing and quantifying molecular goodness-of-fit: small-probe contact dots with explicit hydrogen atoms. J. Mol. Biol 285, 1711–1733. [PubMed: 9917407]

(21). Leaver-Fay A, Tyka M, Lewis SM, Lange OF, Thompson J, Jacak R, Kaufman K, Renfrew PD, Smith CA, Sheffler W, Davis IW, Cooper S, Treuille A, Mandell DJ, Richter F, Ban YE, Fleishman SJ, Corn JE, Kim DE, Lyskov S, Berrondo M, Mentzer S, Popovic Z, Havranek JJ, Karanicolas J, Das R, Meiler J, Kortemme T, Gray JJ, Kuhlman B, Baker D, and Bradley P. (2011) ROSETTA3: an object-oriented software suite for the simulation and design of macromolecules. Methods Enzymol. 487, 545–574. [PubMed: 21187238]

(22). Bazzoli A, Kelow SP, and Karanicolas J. (2015) Enhancements to the Rosetta Energy Function Enable Improved Identification of Small Molecules that Inhibit Protein-Protein Interactions. PLoS One 10, e0140359.

(23). van der Walt S, Colbert SC, and Varoquaux G. (2011) The NumPy Array: A structure for efficient numerical computation. Comput. Sci. Eng 13, 22–30.

(24). Hunter JD (2007) Matplotlib: a 2D graphics environment. Comput. Sci. Eng 9, 90–95.

(25). Zang Q, and Springer TA (2001) Amino acid residues in the PSI domain and cysteine-rich repeats of the integrin beta2 subunit that restrain activation of the integrin alpha(X)beta(2). J. Biol. Chem 276, 6922–6929. [PubMed: 11096074]

(26). Hynes RO (2002) Integrins: bidirectional, allosteric signaling machines. Cell 110, 673–687. [PubMed: 12297042]

(27). Vinogradova O, Velyvis A, Velyviene A, Hu B, Haas T, Plow E, and Qin J. (2002) A structural mechanism of integrin aIIbb3 ″inside-out″ activation as regulated by its cytoplasmic face. Cell 110, 587–597. [PubMed: 12230976]

(28). Bennett JS (2005) Structure and function of the platelet integrin alphaIIbbeta3. J. Clin. Invest 115, 3363–3369. [PubMed: 16322781]

(29). Eng ET, Smagghe BJ, Walz T, and Springer TA (2011) Intact αIIbβ3 integrin is extended after activation as measured by solution X-ray scattering and electron microscopy. J. Biol. Chem 286, 35218−35226.

(30). Beglova N, Blacklow SC, Takagi J, and Springer TA (2002) Cysteine-rich module structure reveals a fulcrum for integrin rearrangement upon activation. Nat. Struct. Biol 9, 282–287. [PubMed: 11896403]

(31). Wang W, Fu G, and Luo BH (2010) Dissociation of the alpha-subunit Calf-2 domain and the beta-subunit I-EGF4 domain in integrin activation and signaling. Biochemistry 49, 10158−10165.

(32). Bury L, Falcinelli E, Chiasserini D, Springer TA, Italiano JE Jr., and Gresele P. (2016) Cytoskeletal perturbation leads to platelet dysfunction and thrombocytopenia in variant forms of Glanzmann thrombasthenia. Haematologica 101, 46–56. [PubMed: 26452979]

(33). Kashiwagi H, Kunishima S, Kiyomizu K, Amano Y, Shimada H, Morishita M, Kanakura Y, and Tomiyama Y. (2013) Demonstration of novel gain-of-function mutations of alphaIIbbeta3: association with macrothrombo-cytopenia and glanzmann thrombasthenia-like phenotype. Mol. Genet. Genomic Med 1, 77–86. [PubMed: 24498605]

(34). Kamata T, Handa M, Sato Y, Ikeda Y, and Aiso S. (2005) Membrane-proximal {alpha}/{beta} stalk interactions differentially regulate integrin activation. J. Biol. Chem 280, 24775−24783.

(35). Xiong JP, Stehle T, Goodman SL, and Arnaout MA (2003) New insights into the structural basis of integrin activation. Blood 102, 1155–1159. [PubMed: 12714499]

(36). Zhu J, Boylan B, Luo BH, Newman PJ, and Springer TA (2007) Tests of the extension and deadbolt models of integrin activation. J. Biol. Chem 282, 11914−11920.

(37). Moreira IS, Fernandes PA, and Ramos MJ (2007) Hot spots–a review of the protein-protein interface determinant aminoacid residues. Proteins: Struct., Funct., Genet 68, 803–812. [PubMed: 17546660]

(38). Singh J, and Thornton JM (1990) SIRIUS. An automated method for the analysis of the preferred packing arrangements between protein groups. J. Mol. Biol 211, 595–615. [PubMed: 2308168]

(39). Mitchell JB, Laskowski RA, and Thornton JM (1997) Non-randomness in side-chain packing: the distribution of interplanar angles. Proteins: Struct., Funct., Genet 29, 370–380. [PubMed: 9365991]

(40). Chakrabarti P, and Bhattacharyya R. (2007) Geometry of nonbonded interactions involving planar groups in proteins. Prog. Biophys. Mol. Biol 95, 83–137. [PubMed: 17629549]

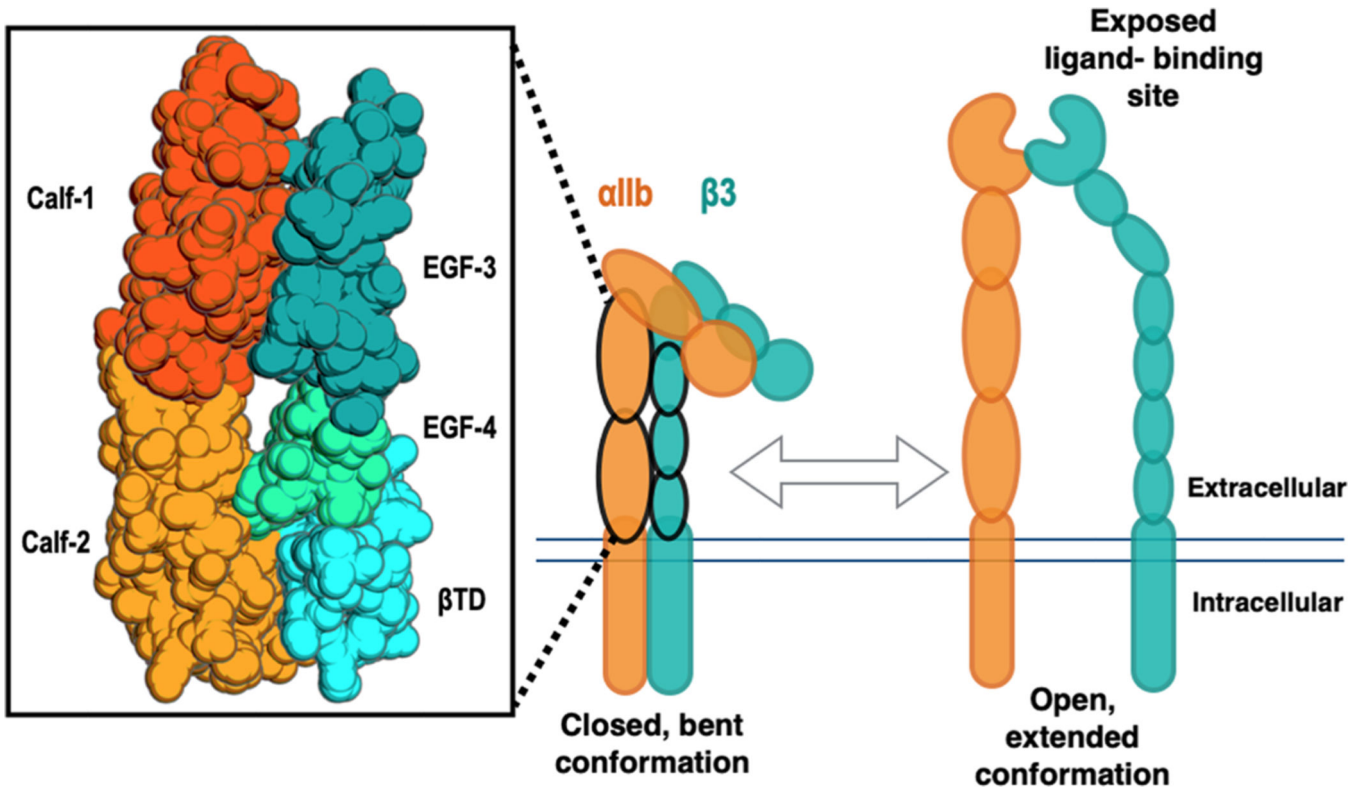

Figure 1.

Model of αIIbβ3 undergoing a global conformational shift between its bent inactive and its extended ligand-binding states. The inset is a space-filling model of the distal αIIbβ3 stalk domains that encompasses αIIb resides 599−959 and β3 residues 483−691[4] and is derived from the Xray crystal structures shown in Protein Data Bank entry 3FCS.

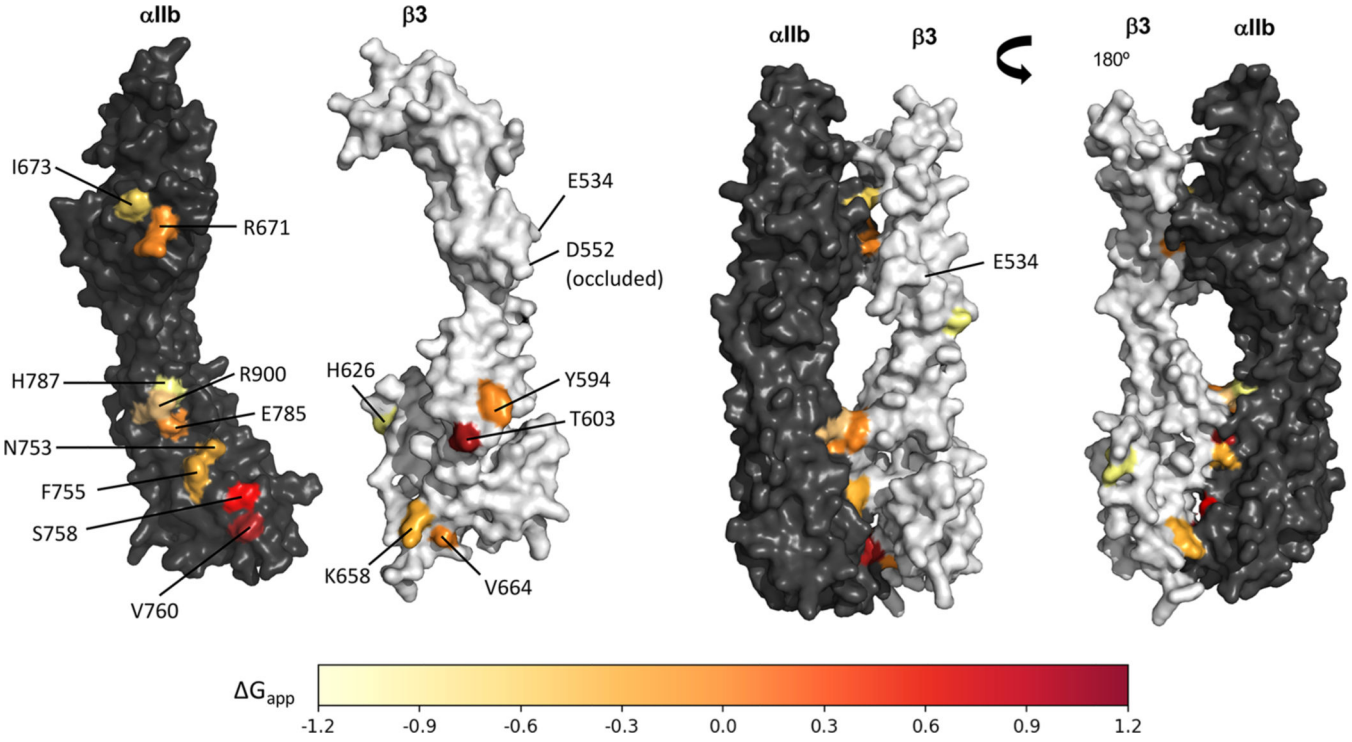

Figure 2.

Mapping of functional hot spots identified by alanine scanning mutagenesis onto the structures of the αIIb and β3 stalk domains. The locations of residues in the distal αIIb and β3 stalk domains for which alanine replacements caused constitutive αIIbβ3 activation were mapped onto the structures for these domains and are color-coded according to the apparent free energy of fibrinogen binding (ΔG_{app}) of their alanine replacement (Table 1), as shown in the heat map below the models.

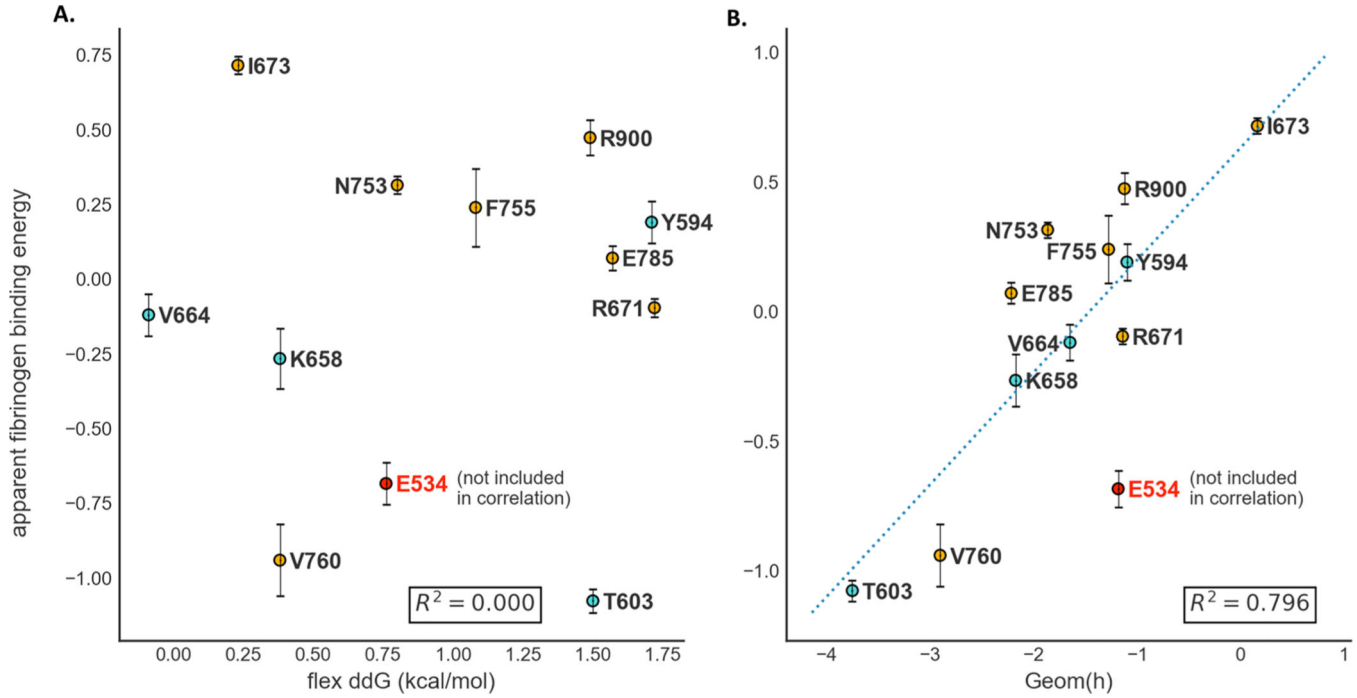

Figure 3.

Correlation between the apparent fibrinogen binding energy of the activating alanine replacements in the αIIb and β3 stalks and (A) the corresponding $\Delta\Delta G$'s predicted by flex ddG or (B) the corresponding Geom(h) scores calculated from the structural bioinformatics analysis. The ΔΔG values predicted by flex ddG are shown in Table 1, and corresponding Geom(h) scores are listed in Table S2. Changes in the apparent energy of fibrinogen binding resulting from the scanning mutagenesis of the αIIbβ3 stalks with alanine replacements were calculated using eq 3. β3 residue E534A was excluded from the correlation because it is not located in the stalk domain interface.

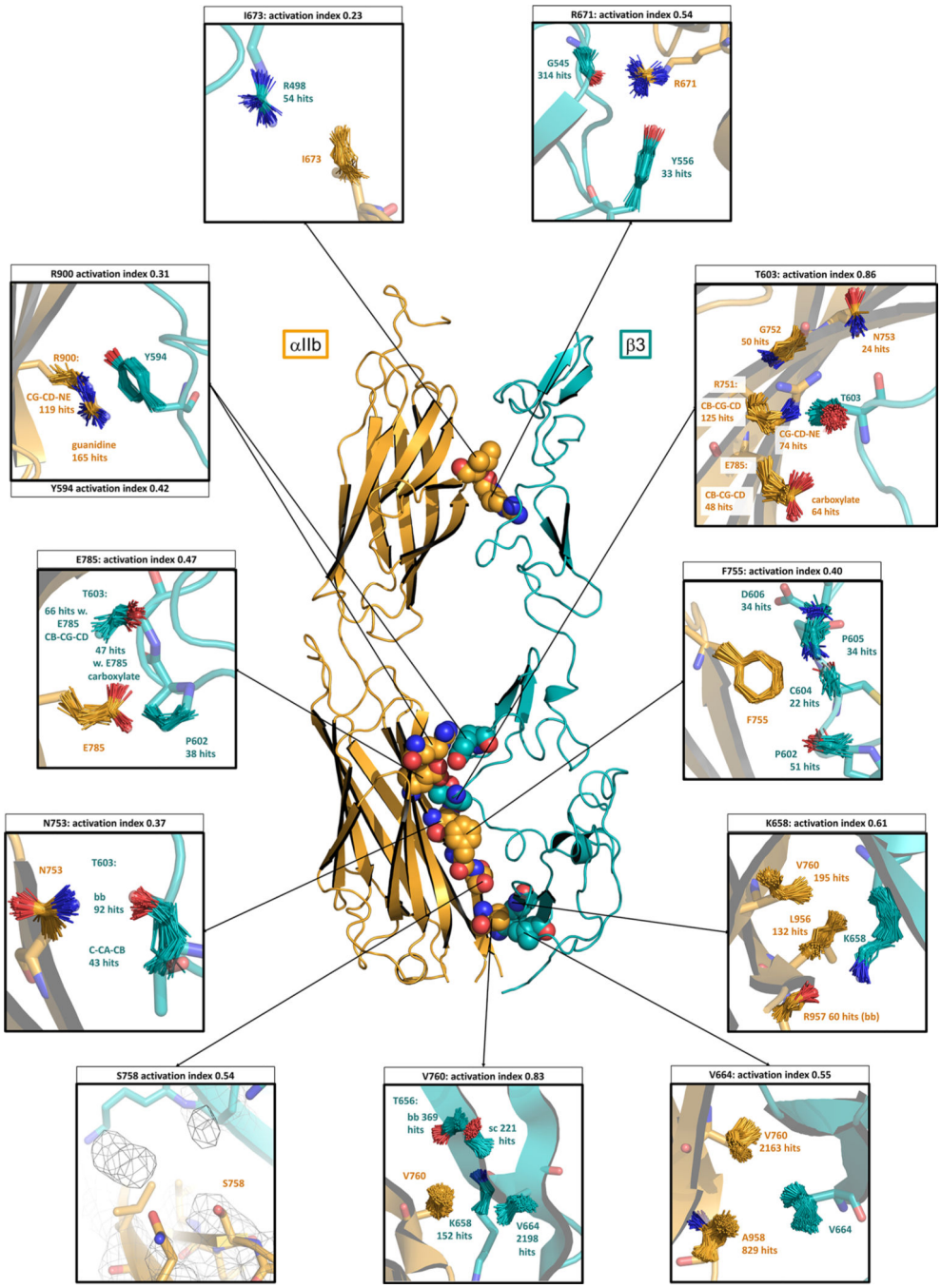

Figure 4.

Favorability of the interaction geometry between αIIb and β3 stalk domains determined from knowledge-based structural bioinformatics. The αIIb stalk is colored orange, and the β3 stalk is colored cyan. Activation index values were derived from Table 1. αIIb or β3 residues and their complementary interacting residues, as well as the number of geometric matches in the PDB, were determined using structural bioinformatics as described in Methods and are listed in Table S2.

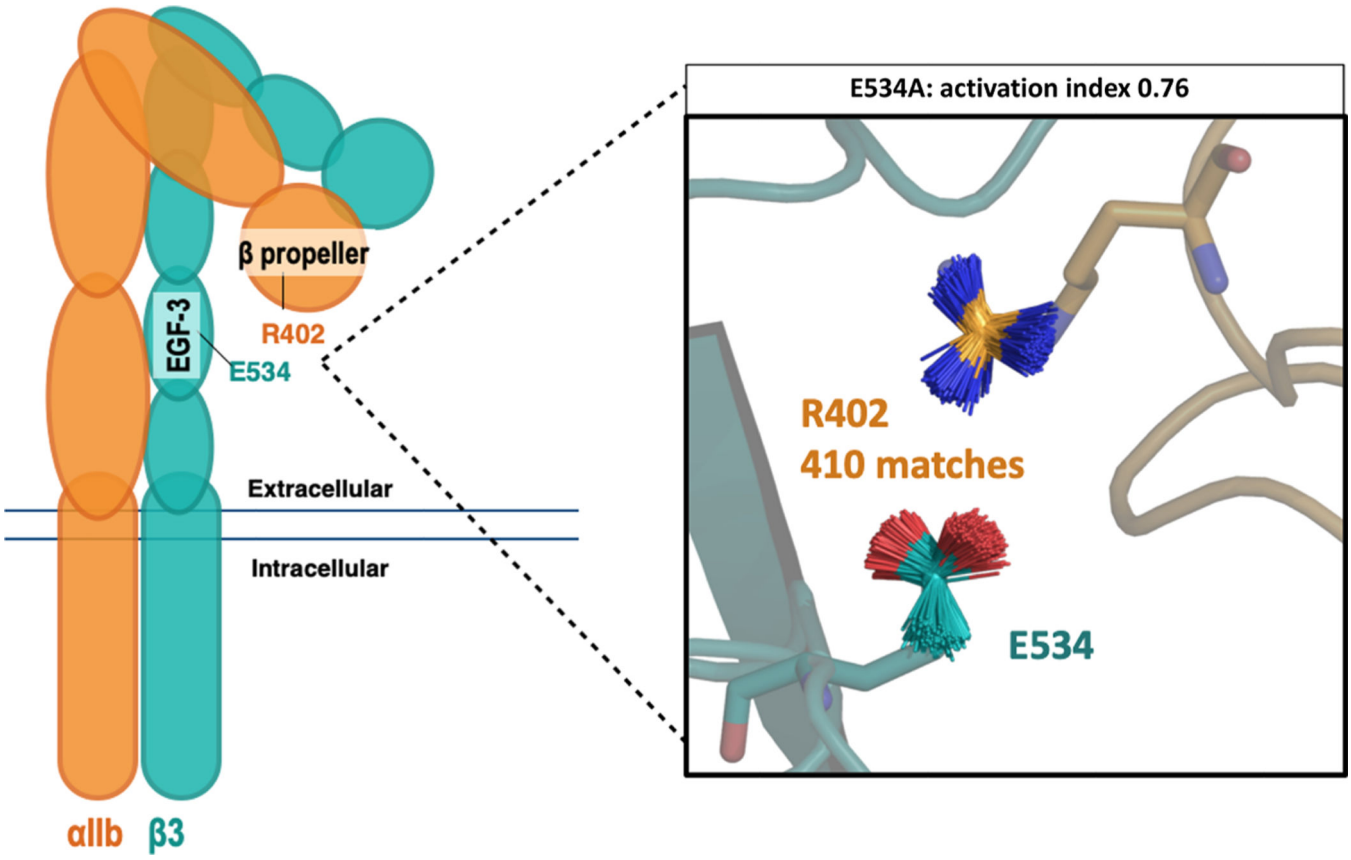

Figure 5.

Alanine replacement of β3 residue E534 causes constitutive αIIbβ3 activation by disrupting the interaction of E534 with αIIb β-propeller residue R402. Replacing predicted β3 residue E534 with alanine causes robust αIIbβ3 activation with an AI of 0.76 (Table 1). However, E534 is not interfacial, but it is in direct contact with αIIb residue R402 located in the αIIb β-propeller domain.

Table 1.

Comparison of Integrin αIIb and β3 Stalk Domain Hot Spots and the αIIbβ3 Activation Index

mutation	subunit	Robetta alanine scanning (kcal/mol)	αIIbβ3 activation index	Rosetta flex ddG (kcal/mol)
F669A	αIIb	0.88	–	0.65
R671A	αIIb	1.53	0.54 ± 0.03	1.72
I673A	αIIb	0.12	0.23 ± 0.03	0.23
N691A	αIIb	0.62	–	2.20
R751A	αIIb	1.49	–	0.65
N753A	αIIb	1.32	0.37 ± 0.03	0.80
F755A	αIIb	1.76	0.40 ± 0.13	1.08
S758A	αIIb	0.56	0.64 ± 0.10	−0.04
V760A	αIIb	0.71	0.83 ± 0.12	0.38
E785A	αIIb	1.20	0.47 ± 0.04	1.57
H787A	αIIb	0.06	0.17 ± 0.02	−0.06
R900A	αIIb	0.54	0.31 ± 0.06	1.49
Q497A	β3	1.98	–	1.86
E534A	β3	0.54	0.76 ± 0.07	0.76
D552A	β3	0	0.17 ± 0.04	0.03
Y556A	β3	0.40	–	0.05
Y594A	β3	0.60	0.42 ± 0.07	1.71
T603A	β3	2.89	0.86 ± 0.04	1.50
D606A	β3	0.71	–	0.42
T609A	β3	1.42	–	0.29
H626A	β3	0	0.19 ± 0.05	0
K658A	β3	0.63	0.61 ± 0.10	0.38
V664A	β3	0.34	0.55 ± 0.02	−0.09